

# Hydrometeor classification with a C-band polarimetric radar

T. Keenan

Bureau of Meteorology Research Centre, Australia

(Manuscript submitted July 2002; revised December 2002)

**An empirically based fuzzy logic microphysical classification scheme is described using C-band polarimetric radar measurements. Polarimetric power and differential phase measurements in both radial and cartesian space are employed to define membership functions in two-dimensional subspaces and are then coupled with a temperature-dependent membership function to classify scattering hydrometeors into one of ten species. Examples of this approach are presented for a tropical thunderstorm observed near Darwin, Australia and for a subtropical severe thunderstorm observed near Sydney, Australia. Examination of these examples shows that realistic results are obtained through this empirically based algorithm.**

## Introduction

The scattering of electromagnetic energy by hydrometeors forms the basis of radar meteorology. Knowledge of hydrometeor types can be very important in particular applications. The occurrence of mixed-phase conditions, especially the melting of snow and ice, impacts on the accuracy of radar-based precipitation estimation and the discrimination of rain and hail is often very important in severe weather warning production. Other applications, described by Straka et al (2000), are linked to the estimation of latent heat release and the initialisation of hydrometeor species in numerical models. Fortunately, the type of hydrometeor responsible for the scattering of electromagnetic energy can produce significantly different characteristics of the returned radar signal, especially for multiparameter radars.

This paper follows studies by Aydin et al. (1986), Straka and Zrnic (1993), Höller et al. (1994) and Vivekanandan et al. (2000) to further show that multiparameter radars have considerable potential to

identify bulk hydrometeor types. The work was prompted in part by a primary application of the Bureau of Meteorology Research Centre (BMRC) C-band polarimetric radar (CPOL), described by Keenan et al. (1998), in the validation of the National Aeronautics and Space Administration (NASA) and National Space Development Agency of Japan (NASDA) Tropical Rainfall Measuring Mission (TRMM) products. The accuracy of TRMM algorithms is in part determined by the hydrometeor species and physical validation of these algorithms requires information on the vertical distribution of hydrometeors above the melting level, especially in the 'mixed-phase' region.

This paper first describes the measurements undertaken by CPOL, summarises the microphysical classification procedure and then presents examples of the classification procedure in very different tropical and subtropical environments. This demonstrates the apparent robustness of the approach, a fact supported by routine use of the techniques in TRMM Ground Validation (GV) and the World Weather Research Programme Forecast Demonstration Project (Keenan et al. 2002) undertaken in Sydney, Australia. This

---

*Corresponding author address:* T. Keenan, BMRC, GPO Box 1289K, Melbourne, Vic. 3001, Australia.

work extends previously reported development of this type undertaken predominantly at S-band. At C-band additional problems arise associated with the increased magnitude of attenuation and Mie scattering effects. In this study, attenuation that occurs in rain is corrected for using a multiparameter polarimetric-based attenuation correction procedure.

## CPOL polarimetric variables and processing procedures

CPOL transmits electromagnetic energy on a pulse-by-pulse basis in linear horizontal and vertically polarised states and then measures the corresponding power (co-polar state) with a single receiver. The variables available for the microphysical classification include the horizontal radar reflectivity ( $Z_{HH}$ ) defined as:

$$Z_{HH} = \frac{\lambda^5}{\pi^5 |k|^2} \int \sigma_{HH}(D) N(D) dD \quad \dots 1$$

where  $\sigma_{HH}$  is the radar cross-section at the horizontal (H) copolar state,  $N(D)$  is the particle size distribution,  $\lambda$  is the radar wavelength, and  $k = (\epsilon - 1) / (\epsilon + 1) - 1$ , with  $\epsilon$  being the complex relative permittivity of the particle. Raindrops are distorted by aerodynamic forces such that the larger the drop the more it takes on an oblate spheroid shape having a mean axis ratio less than one, as described by Pruppacher and Pitter (1971) and Beard and Chuang (1987). Drops less than 0.3 mm in diameter are essentially spherical, whereas drops near 4 mm in diameter have a mean axis ratio near 0.8. Thus vertically polarised radar reflectivity ( $Z_{VV}$ ) is less than  $Z_{HH}$ . In addition, ice particles have a lower dielectric constant (5-20 per cent less depending on ice density) than water, hence ice has an intrinsically lower reflectivity (6-13dB) for an equivalent size particle.  $Z_{HH}$  is impacted by radar power calibration and propagation (attenuation) effects. This is especially the case at C-band in heavy rain and particularly where large drops are present.

The second variable measured by CPOL is the differential reflectivity  $Z_{DR}$  defined as:

$$Z_{DR} = 10 \log \left( \frac{Z_{HH}}{Z_{VV}} \right) \quad \dots 2$$

Following Jameson (1983),  $Z_{DR}$  is interpreted in terms of the reflectivity weighted mean axis ratio of the precipitation particle and for oblate raindrops is  $>0$ . It is useful in discriminating oblate raindrops from spherical particles e.g., a minimum in  $Z_{DR}$  (assuming spherical hail) with an elevated maxima of  $Z_{HH}$  has been interpreted in terms of hail (Bringi et al. 1986;

Illingworth et al. 1987). If the axis ratio of the hydrometeor is greater than one, then  $Z_{DR} < 0$  as in the case of ice particles aligned vertically by electric fields. At C-band,  $Z_{DR}$  is seriously affected by differential attenuation and Mie scatter effects.

The zero lag cross-correlation coefficient ( $\rho_{HV}(0)$ ) is also available and for backscatter amplitudes  $S_{HH}$  and  $S_{VV}$  is related to the cross-correlation coefficient  $\rho_{HV}$  as follows

$$\rho_{HV} = \frac{\int \sigma_{HH}^* S_{VV} N(D) dD}{[\int \sigma_{HH}^2 N(D) dD]^{0.5} [\int \sigma_{VV}^2 N(D) dD]^{0.5}} \quad \dots 3$$

and  $\rho_{HV} = \rho_{HV}(0) e^{i\delta}$  where  $\rho_{HV}(0)$  is the magnitude of  $\rho_{HV}$  and  $\delta$  is the backscatter differential phase shift. The correlation decreases if the vertical and horizontal components of the scattered energy are not affected in the same way. Physical interpretations of this effect are in terms of particle reorientation, changes in particle numbers and mixtures of hydrometeor phase in the scatter volume are discussed by Straka et al. (2000). This variable is relatively independent of radar calibration and immune to propagation effects. Non-zero values of  $\delta$  imply Mie scattering (typically when hydrometeor size is  $>0.1$  the radar wavelength).

The two-way differential propagation phase shift  $\Phi_{DP}$  between horizontal and vertical polarised energy is also measured and is defined as

$$\Phi_{DP} = 2 \int_{r_1}^{r_2} K_{DP}(r) dr \quad \dots 4$$

between ranges  $r_1$  and  $r_2$ , where the specific differential phase  $K_{DP}$  is defined as

$$K_{DP} = \frac{2\pi}{k_0} \text{Re} \int [f_{HH} - f_{VV}] N(D) dD \quad \dots 5$$

given  $k_0$  is the free space propagation constant and  $f_{HH}$  and  $f_{VV}$  are forward scatter amplitudes. A horizontally polarised wave encountering horizontally oriented particles produces a large phase shift and propagates slower than the vertically polarised wave. This differential phase shift enables isotropic and anisotropic hydrometeors to be distinguished given that in a statistical sense isotropic or spherical hydrometeors produce the same phase shift. It increases with increased oblateness and dielectric constant.  $K_{DP}$  is almost linearly related to rain rate and ice water content. The differential phase shift is relatively easy to measure, especially at C-band where phase shifts are larger than at S-band. It is independent of radar power calibration, less sensitive to drop size distribution changes and less impacted by beam blockage effects. However, estimation of  $K_{DP}$  from  $\Phi_{DP}$  is affected by Mie scattering effects. This

may be indicated by the presence of an associated backscatter differential phase ( $\delta$ ). Such effects are more likely at C rather than S-band

Microphysical interpretation of the above variables has been developing through numerous observational and modelling studies. A phase space type interpretation of the polarimetric variables is usually employed as discussed above. Discrimination between ice and liquid is possible using  $Z_{HH}$  and  $K_{DP}$  given that  $K_{DP}$  is affected only by the anisotropic hydrometeors (rain), as discussed by Lopez and Aubagnac (1997). Vivekanandan et al. (1994) show how  $Z_{HH}$ ,  $Z_{DR}$  and  $K_{DP}$  together can be employed to infer rain and the presence of a mixed-phase.  $Z_{HH}$  and  $Z_{DR}$  can infer or discriminate the presence of pristine ice and snow. These types of studies have been further extended by Straka and Zrníc (1993), Vivekanandan et al. (2000) and Liu and Chandrasekar (2000).

### Preprocessing of polarimetric variables

As mentioned above, any radar bias or attenuation can produce measured polarimetric variables with errors, and as a result influence the veracity of the classification results. Given a C-band radar is more susceptible to such propagation effects, a multi-pronged approach is employed in this paper to minimise such problems. First the CPOL data are subjected to self-consistency checks to minimise the potential impact of calibration errors\* especially on power based measurements such as  $Z_{HH}$  and  $Z_{DR}$ . Secondly,  $Z_{HH}$  and  $Z_{DR}$  are corrected for attenuation and differential attenuation in rain following Bringi et al. (2002). These techniques are described in the Appendix. Thirdly, a fuzzy logic-based classification procedure is employed to undertake the actual hydrometeor classification. This approach potentially reduces the impact of uncertainties in the polarimetric variables in the classification procedure. Given the  $K_{DP}$  is not measured directly by the radar it must first be estimated from the range derivative of the measured  $\Phi_{DP}$ . The finite impulse response method of Hubbert and Bringi (1995) is employed here to derive a filtered version of  $\Phi_{DP}$  enabling estimation of  $K_{DP}$  and any backscatter differential phase shift. The algorithm is configured to employ nine successive range bins. The respective bin resolution was 150 m for Range Height Indicator (RHI) and 300 m for Plan Position Indicator (PPI) radar scans employed in this paper.  $K_{DP}$  was estimated from the range derivative of the filtered  $\Phi_{DP}$  but

with the additional constraint that  $Z_{HH}$  be  $> 15$  dBZ.

### Microphysical classification process

Various techniques have been employed to undertake hydrometeor classifications based on information of the type presented in Table 1. They range from manual lookup table approaches generally employed in one-off diagnostic studies of the type undertaken by Carey and Rutledge (1996), decision tree methods of the type employed by Straka and Zrníc (1993) and Höller (1995); fuzzy logic-based approaches as undertaken by Vivekanandan et al. (2000), Zrníc et al. (2001) and a neural network and fuzzy logic combination presented by Liu and Chandrasekar (2000).

In this paper the hydrometeor classification procedure is a fuzzy logic approach given that strict well-defined physically based rules or analytical expressions are not available or known. Nevertheless, the ranges of variables shown in Table 1 do have some physical basis given they are built on extensive modelling studies, observations and theory. However, it is possible to obtain more than one outcome for each input and it must be recalled that the radar data are not error free. Hence application of the fuzzy logic approach would seem to offer certain practical advantages as discussed by Mendel (1995). However, even though corrections have been undertaken to assure data quality, the potential certainly exists for misclassifications based on the inherent uncertainties in the data and the empirical nature of the classification procedures. Of course alternative approaches do exist and future work could explore such approaches.

Herein, the phase space shown in Table 1 linking polarimetric variables to microphysical variables first outlined by Doviak and Zrníc (1993) and later refined by Straka et al. (2000) is employed\*. The ten hydrometeor species considered are drizzle, rain, dry low density snow, high density snow crystals, wet melting snow, dry graupel, small wet hail, large wet hail and a rain hail mixture. An environmental temperature dependent constraint is also employed to further refine the classification process.

The fuzzy logic approach reaches specific decisions by first undertaking fuzzification of the measurements by converting them to sets defined by a membership function. The membership function defines the degree to which the fuzzy variable belongs to a particular set, i.e., the degree to which a polarimetric variable is related to a particular hydrometeor species. Inferences are then made on the strength of the various rules. In this case, inferences are made on the likelihood that each species is present

\* This check follows normal engineering-based electronic and absolute calibration procedures on CPOL described by Keenan et al. (1998).

\* Note only the  $K_{DP}$  ranges have been modified to reflect the operation of the classification procedure at C-band.

**Table 1. Ranges of polarimetric variables and temperature for various hydrometeor species.**

	$Z_{HH}$ (dBZ)	$Z_{DR}$ (dB)	$\rho_{HV}(0)$	$K_{DP}$ (deg km <sup>-1</sup> )	Temperature (°C)
Drizzle	10-25	0.2 to 0.7	>0.97	0 to 0.06	>-10
Rain	25 to 60	0.5 to 4	>0.95	0 to 20	>-10
Snow (dry, low density)	-10 to 35	-0.5 to 0.5	>0.95	-1 to 1	<0
Snow* (dry, high density)	-10 to 35	0.0 to 1	>0.95	0 to 0.4	<0
Snow (wet, melting)	20 to 45	0.5 to 3	0.5 to 0.9	0 to 1	0 to 5
Graupel, dry	20 to 35	-0.5 to 1	>0.95	0 to 1	<0
Graupel, wet	30 to 50	-0.5 to 2	>0.95	0 to 3	-15 to 5
Hail, small < 2 cm wet	50 to 60	-0.5 to 0.5	0.92 to 0.95	-1 to 1	-15 to 20
Hail, large > 2 cm wet	55 to 65	-1 to 0.5	0.90 to 0.92	-1 to 2	-25 to 20
Rain and hail	45 to 80	-1 to 6	>0.9	0 to 20	-10 to 25

based on the observed values of the polarimetric variables and the environmental temperature. An aggregation of the inferences is then undertaken to define a most likely or overall result by picking the maximum confidence factor.

Following the above general principles, the classification procedure is based on the use of fuzzy logic membership functions with a four step process to define hydrometeor species ( $j=1-10$ ). The four steps are:

- (a) The probability ( $P_j^T$ ) of each hydrometeor species being present is derived based on the environmental temperature of the radar sample volume,

$$P_j^T = P_j(T_j^{lower}, T_j^{upper}, T) \quad \dots 6$$

where  $P_j(T_j^{lower}, T_j^{upper}, T)$  is the temperature membership function,  $T$  is the temperature of the sample volume, and  $T_j^{lower}$  and  $T_j^{upper}$  represent temperature bounds from Table 1 considered consistent with the physical existence of the various hydrometeor species.

- (b) The probability ( $P_j^R$ ) of each species is deduced based on the polarimetric variables  $R_k$  (where  $k=1, 4$  corresponds to  $Z_{HH}$ ,  $Z_{DR}$ ,  $K_{DP}$  and  $\rho_{HV}(0)$ ) using the ranges provided in Table 1.

$$P_j^R = \sum_k W_k P_j^k(R_k^{lower}, R_k^{upper}, R_k) / \sum_k W_k \quad \dots 7$$

where  $W_k$  is a weighting function for each polarimetric variable (all equal to one in this case).

- (c) The above two probabilities are then combined to estimate  $P_j$  the aggregated or total probability of each species,

$$P_j = P_j^T + P_j^R \quad \dots 8$$

- (d) If the maximum confidence value  $P_j$  meets the following criterion

$$| \max(P_j) - \bar{P} | \geq 1.75\sigma_p \quad \dots 9$$

where  $\sigma_p$  is the standard deviation of the hydrometeor class probabilities, class  $j$  is assigned. Hence missing classifications are evident in low confidence situations.

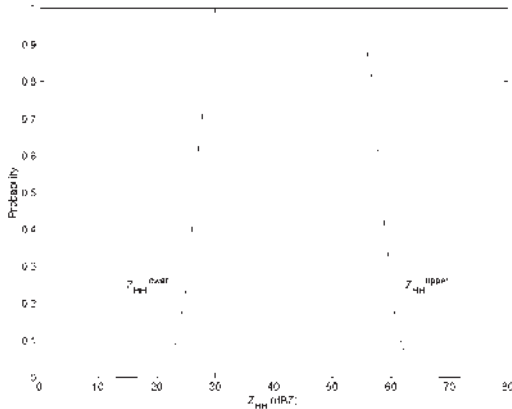
A Gaussian Bell function (similar to the beta functions used by Liu and Chandrasekar, 2000) structured with five per cent percentile tails is employed for assigning class membership probabilities, as illustrated in Fig.1, for the case of rain based on  $Z_{HH}$ . The choice of the Gaussian Bell classification function was somewhat arbitrary. The approach undertaken here is similar to that used by Zrnice et al. (2001), where linear segment membership functions were employed.

The fuzzy logic classification procedure is undertaken either on a gate by gate basis in radial radar space (for RHI scans) or on a cartesian grid (for volume scans).

As discussed above, the nearest available temperature sounding is employed in this algorithm. However, the crucial temperature measurement is the height of the melting level and in principle this could be defined from the radar data by measuring the height of the radar 'bright band'. This can be inferred by reflectivity profiles and/or by values of polarimetric variables e.g., decreased  $\rho_{HV}$ . It should be noted that Zrnice et al. (2001) have tested the sensitivity of such 'fuzzy logic' classifications to the number of polarimetric variables and the temperature information made available to the scheme. Reflectivity and differential reflectivity were found to have the great-

\* Rimed and aggregated snow.

**Fig. 1** An example of the Gaussian membership probability function employed for class assignments. In this case the rain class assignment based on  $Z_{HH}$  is shown. Dotted vertical lines indicate  $Z_{HH}$  limits given in Table 1.



est discriminating power. Absence of the temperature information also degraded the classification process. These issues are not addressed in this paper.

### Sample classifications

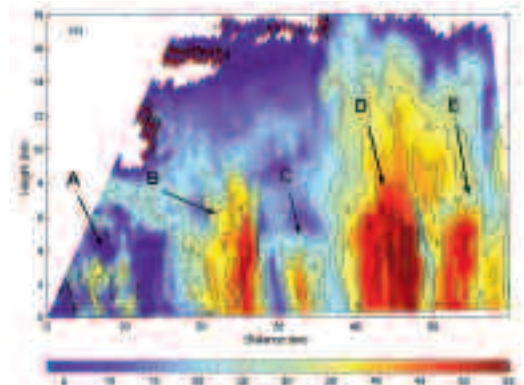
Results from applying the classification scheme at tropical and subtropical locations are now provided. The classification algorithm is identical in both cases. The only change was the use of the nearest available rawinsonde sounding to provide environmental temperature information.

#### Deep tropical convection near Darwin, Australia

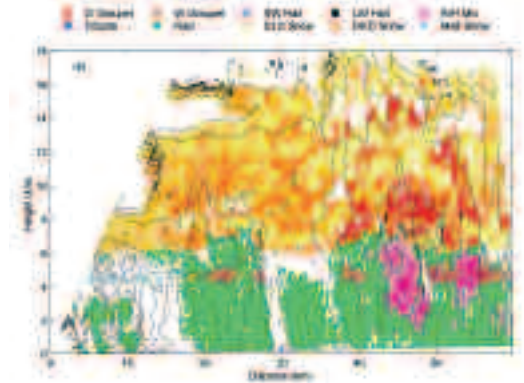
An RHI through a deep convective system with five cells (A,B,C,D and E) of various depths embedded in an anvil, observed at Darwin, is shown in Fig. 2. The classification scheme shows overall transition from rain at low levels to an anvil dominated by dry low density snow. There is ample evidence for dry high density snow in the anvil especially in the region of convective cores (e.g. B, C, D and E). The deepest and most intense convective cell denoted D, shows dry graupel above the convective core, mostly below 9 km height but within patches at heights from 12-15 km. Wet graupel and a rain hail mixture (in the region of maximum radar reflectivity) are evident mainly in the 3-5 km height range in cells D and E. Rain is diagnosed below 4 km height and in all cells there is evidence for supercooled rain water between 5 and 6 km height (implied from  $Z_{DR}$  measurements but not shown). Near and just below the melting level (5 km height), there is evidence of wet graupel (in the con-

**Fig. 2** RHI-based vertical cross-section through a tropical thunderstorm complex observed at 0728 UTC 3 February 2000 near Darwin, Australia. (a) Radar reflectivity (dB) with cells A-E (see text) indicated and (b) hydrometeor types derived from the microphysical classification system.

(a)



(b)



vective regions) and melting snow (in the stratiform areas) consistent with expected microphysical processes.

Within the mixed phase region there is considerable variability as would be expected. Examination of other such situations shows that the scheme does experience difficulty in these regions. Use of the linear depolarisation ratio ( $L_{DR}$ ) which is the ratio of the cross-polar to co-polar power could be useful.  $L_{DR}$  values are small for rain (and dry ice) but larger for wet ice particles such as hail, melting aggregates and wet graupel. However,  $L_{DR}$  is difficult to measure given the relatively small signal levels of the co-polar

energy. Depolarisation effects can also be significant.

At present CPOL does not have the capability to undertake the  $L_{DR}$  measurements.

### Subtropical severe thunderstorm observed near Sydney, Australia

A vertical cross-section derived from a volume scan through a super cell tornadic storm observed near Sydney on 3 November 2000 is shown in Fig. 3. Hail was observed at the ground from this storm over the period 0345-0610 UTC. The maximum hail size observed was 47 mm diameter at a time near 0500 UTC. In this case, the algorithm was invoked using data interpolated to a cartesian grid with grid resolution of 0.5 km in the horizontal and 0.25 km in the vertical. The microphysical classification scheme was applied in cartesian space.

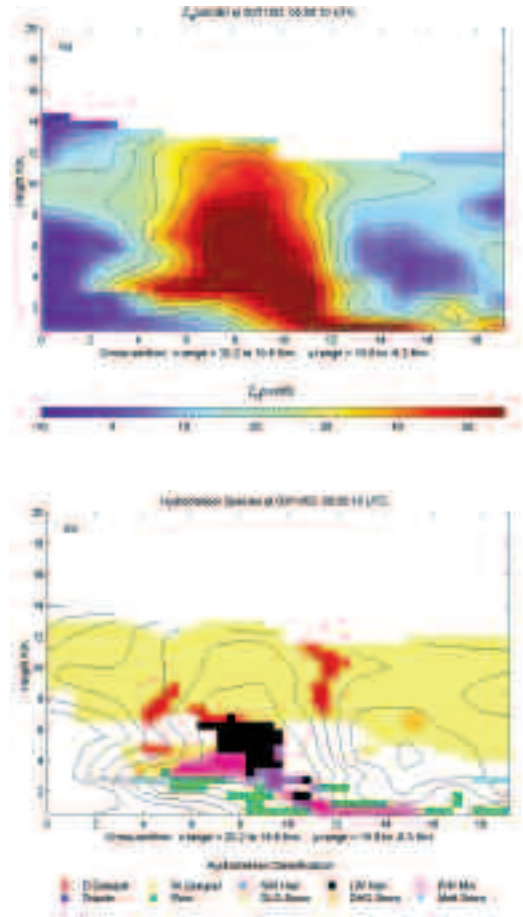
As shown in Fig. 3a, the storm in this case is much shallower than the tropical event presented previously (storm top near 14-15 km versus 18 km in Fig. 2). This storm exhibited an intense elevated reflectivity maximum ( $> 60$  dBZ) at a height of 6 km with a secondary maximum near the ground ( $x=12-14$  km in Fig. 3(a)). The elevated reflectivity maximum is classified as a mixture of large wet hail and smaller wet hail. Below this are mixtures of rain-hail and melting snow presumably formed as a result of melting within the falling ice and snow. On the fringes of the reflectivity maximum area, in the weaker echo region, near  $x=4-7$  km, rain, melting hail and wet graupel are evident. Presumably this is the updraft region where rain and water are present before recycling has enabled significant hail growth. The reflectivity maximum near ground level is classified as being a mixture of rain and hail at this particular time. This is consistent with the observed reports of hail although as evident in Fig. 3, there is considerable spatial variability in the hail at ground level.

## Summary

A simple empirically based fuzzy logic microphysical classification scheme has been described based on the use of C-band polarimetric radar measurements. Two dimensional sub spaces of  $Z_{HH}$ ,  $Z_{DR}$ ,  $\rho_{HV}(0)$  and  $K_{DP}$  coupled with a temperature dependent membership function form the basis for classifying ten hydrometeor species. Initial results presented here show that plausible results are obtained. However, the technique does experience some difficulty in the mixed phase region given the ambiguous nature of the radar returns and

**Fig. 3** Vertical cross-section derived from a CPOL volume scan through a severe thunderstorm observed at 0500 UTC 3 November 2000 near Sydney, Australia. (a) Radar reflectivity and (b) hydrometeor types derived from the microphysical classification system.

(a)



hydrometeors.

The technique is now being implemented for real-time operation as part of CPOL's ground validation activities. Web based products will be derived and available immediately for TRMM investigators.

## Acknowledgments

This work was prompted following discussions with Dusan Zrnica during a visit to BMRC. Operation of the

CPOL radar was made possible through the combined efforts of engineering staff at the Bureau of Meteorology and in particular Mr Ken Glasson.

## Appendix

### Self-consistency approach to calibration and corrections for attenuation in rain

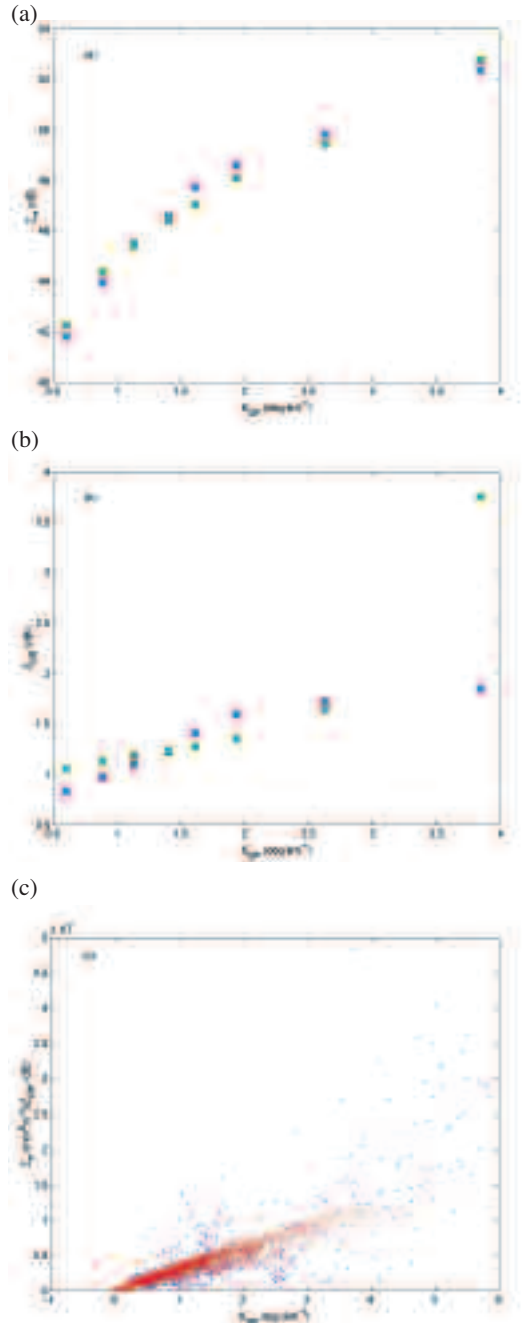
For a given raindrop size distribution (RSD) and raindrop axial ratio (RAR), systematic relations of the form  $K_{DP}(Z_H, Z_{DR})$ ,  $K_{DP}(Z_{HH})$  and  $K_{DP}(Z_{DR})$  exist. Gorgucci et al. (1999) proposed using the self consistency of such independent phase and power-based measurements to calibrate polarimetric radars. In essence, the ‘intrinsic’ or expected ‘theoretical’ relations between the polarimetric variables, derived from scattering simulations based on assumed RSDs are compared to radar-observed or measured relations between polarimetric variables. This general approach is employed in this paper and is now described.

T-matrix scattering simulations formulated following Barber and Yeh, (1975) and based on 8046 one minute RSDs measured at Darwin, Australia were employed to derive empirical relations of the form  $K_{DP}(Z_{HH})$  and  $K_{DP}(Z_{DR})$ . The sensitivity of these relations to different RSDs has been investigated using data from Dongsha Is, located in the South China Sea and from the subtropical regime of Sydney, Australia. Differences from RSD are found to be insignificant in the context of this work. For the purposes of these calculations, the New Raindrop Axial Ratio (NR) of Keenan et al. (2001) has been employed given its apparent success in removing biases in rain rate studies undertaken by May et al. (1999). For the purposes of this paper, probability matching methods were employed to derive theoretical  $K_{DP}(Z_{HH})$  and  $K_{DP}(Z_{DR})$  relations. These two relations are shown in Fig. A1(a) and (b) in blue.

Each volume scan of CPOL data is subjected to a similar analysis. Percentile values of radar observed  $Z_{HH}$ ,  $Z_{DR}$  and  $K_{DP}$  derived from the ‘raw’ radial radar space are then matched for the ‘observed’  $K_{DP}(Z_{HH})$  and  $K_{DP}(Z_{DR})$  relations. Examples of these relations are also shown in Fig. A1(a) and (b) in green. At the observed  $K_{DP}$  percentile values, the corresponding  $Z_{HH}$  and  $Z_{DR}$  values are interpolated from the so called ‘theory’ values of  $K_{DP}(Z_{HH})$  and  $K_{DP}(Z_{DR})$ . Mean differences are then deduced between the radar observed and the theoretically-derived  $Z_{HH}$  and  $Z_{DR}$  values. These values are employed as a calibration mean offset in each variable.

For the purposes of the algorithm, radar variables considered representative of rain are required to satisfy the following criteria:  $K_{DP} > 0.25 \text{ deg km}^{-1}$ ,  $Z_{HH} > 37.5$ ,  $\rho_{HV}(0) > 0.90$ , with the temperature of the sam-

**Fig. A1** Example of self-consistency tests used to calibrate CPOL for 0728 UTC 3 February 2000. Comparison of 15-85 percentile values of CPOL radar observed and RSD derived for  $Z_{HH}(K_{DP})$  and  $Z_{DR}(K_{DP})$  in (a) and (b) respectively. Radar observed values in green and RSD values from Darwin-based scattering simulations in blue. (c) A comparison of  $Z_{HH}/Z_{DR}(K_{DP})$  after offsets applied. Radar observed values in blue and RSD data in red.



ple volume  $>5^{\circ}\text{C}$  (taken from the closest and most recent atmospheric rawinsonde sounding). Note the variable thresholds are different from those in Table 1 and are employed to ensure significant phase shifts are being measured. This reduces the impact of noisy data in the statistical analysis. A temperature threshold is employed to obtain observed polarimetric variables representing the 'rain only' regime, consistent with the empirical RSD deduced rain relations. For the algorithm to be invoked,  $N$  the total number of points satisfying the above criteria must be  $> 500$ . Typical values for the  $Z_{HH}$  offset range are from  $-2$  to  $2$  and  $Z_{DR}$  from  $-0.5$  to  $0.5$  dB.

The example shown in Fig.A1 produced a  $Z_{HH}$  bias of  $-2$  dB and a rather large  $Z_{DR}$  bias of  $-1$  dB. A comparison of the corrected variables (blue) with those deduced from the RSD data (red) is shown in Fig. A1(c) employing the functional form  $Z_{HH}/Z_{DR}(K_{DP})$ . As evident in Fig. 1(c), even though  $K_{DP}$ ,  $Z_{DR}$  and  $Z_{HH}$  are not truly independent this approach does give corrected values consistent with the theoretical expectations.

Attenuation of C-band radio waves by heavy precipitation can cause significant modification to observed  $Z_{HH}$  and  $Z_{DR}$  values as shown by Carey et al. (2000) and is sensitive to RSD, temperature and drop shape. Attenuation corrections are available with polarimetric radars assuming changes of  $Z_{HH}$  and  $Z_{DR}$  due to attenuation are linearly related to  $\Phi_{DP}$  as described by Bringi et al. (1990). In this case, the rain attenuation correction procedure follows the method of self-consistency with constraints developed by Bringi et al. (2002). This technique extends and combines those proposed by Testud et al. (2000). It is assumed that horizontal attenuation  $A_H$  is linearly related to  $K_{DP}$  and  $Z_{DR}$  in the form  $A_H = \alpha K_{DP}$ . As shown by Carey et al. (2000),  $\alpha$  can vary considerably given the particular RSD encountered. An optimal value of  $\alpha_{opt}$  is derived by matching the observed  $\Phi_{DP}$  with that reconstructed from assuming a power relation between  $A_H$  and  $Z_{HH}$ .

For the differential attenuation, it is assumed that  $A_{DP}$ , the specific attenuation, is specifically related to  $A_H$  via a relation ( $A_{DP} = (\beta/\alpha_{opt}) A_H$ ). Given,  $Z_H(r_m)$ , where  $r_m$  is the range at the far side of a cell, is already corrected for attenuation,  $Z_{DR}(r_m)$  can be established and  $Z_H(r_m)$  and  $Z_{DR}(r_m)$  constrained in a consistent manner. The  $\beta$  value is adjusted iteratively along the ray to produce  $Z_{DR}(r_m)$  within a prescribed tolerance.

Of course these attenuation procedures strictly apply to rain. No attempt has been made to correct for attenuation associated with other hydrometeors e.g.,

hail. It should be noted that the pre-processing including extraction of variables, attenuation correction is undertaken in radial radar space.

## References

- Aydin, K., Seliga, T.A. and Balaji, V. 1986. Remote sensing of hail with a dual polarization radar. *Jnl Clim. appl. Met.*, 25, 75-1484.
- Barber, P. and Yeh, C. 1975. Scattering of electromagnetic waves by arbitrarily shaped dielectric bodies. *Appl. Opt.*, 14, 2864-72.
- Beard, K. and Chuang, D. 1987. A new model for the equilibrium shape of raindrops. *J. Atmos. Sci.*, 44, 1509-24.
- Bringi, V.N., Vivekanandan, J. and Tuttle, J. 1986. Multiparameter radar measurements in Colorado convective storms Part II: Hail detection studies. *J. Atmos. Sci.*, 43, 2564-77.
- Bringi, V.N., Chandrasekar, V., Balakrishnan, N. and Zrnica, D.S. 1990. An examination of propagation effects in rainfall on radar measurements at microwave frequencies. *J. Atmos. Oceanic Technol.* 7, 829-40.
- Bringi, V.N., Keenan, T. and Chandrasekar, V. 2002. Correcting C-band radar reflectivity and differential attenuation: a self-consistent method with constraints. *IEEE Trans. Geoscience and Remote Sensing*, 39, 1906-15.
- Carey, L.D. and Rutledge, S.A. 1996. A multiparameter radar case study of the microphysical and kinematic evolution of a lightning producing storm. *Met. Atmos. Phys.*, 59, 33-64.
- Carey, L.D., Rutledge, S.A., Ahijevych, D. and Keenan, T.D. 2000. Correcting propagation effects in C-band polarimetric radar observations of tropical convection using differential propagation phase. *Jnl appl. Met.*, 39, 1405-33.
- Doviak, R.J. and Zrnica, D.S. 1993. *Doppler radar and weather observations*. Academic Press, San Diego, CA, 562pp.
- Gorgucci, E., Scarchilli G. and Chandrasekar, V. 1999. A procedure to calibrate multiparameter weather radar using properties of the rain medium. *IEEE Transactions on Geoscience and Remote Sensing*, 37, 269-76.
- Höller, H., Bringi, V.N., Hubbert, J., Hagen, M. and Meischner, P.F. 1994. Life cycle and precipitation formation in a hybrid type hailstorm revealed by polarimetric and Doppler radar measurements. *J. Atmos. Sci.*, 51, 2500-22.
- Höller, H. 1995. Radar-derived mass-concentrations of hydrometeors for cloud model retrievals. *Preprints, 27th Conf. On Radar Meteorology*, Vail, CO, Amer. Meteor. Soc., 453-4.
- Hubbert, J. and Bringi, V.N. 1995. An iterative filtering technique for the analysis of copolar differential phase and dual-frequency radar measurements. *J. Atmos. Oceanic Technol.*, 12, 643-8.
- Illingworth, A.J., Goddard, J.W.F. and Cherry, S.M. 1987. Polarization radar studies of precipitation development in convective storms. *Q. Jl R. Met. Soc.*, 113, 469-89.
- Jameson, A.R. 1983. Microphysical interpretation of multiparameter radar measurements in rain. Part I: Interpretation of polarization measurements and estimation of raindrops shapes. *J. Atmos. Sci.*, 40, 1792-802.
- Keenan, T., Glasson, K., Cummings, F., Bird, T.S., Keeler, J. and Lutz, J. 1998. The BMRC/NCAR C-band polarimetric radar system. *J. Atmos. Oceanic Technol.*, 15, 871-86.
- Keenan, T.D., Carey, L.D., Zrnica, D.S. and May, P.T. 2001. Sensitivity of 5-cm wavelength polarimetric radar variables to raindrop axial ratio and drop size distribution. *Jnl appl. Met.*, 40, 526-45.
- Keenan, T., Joe, P., Wilson, J., Collier, C., Golding, B., Burgess, D., May, P., Pierce, C., Bally, J., Crook, A., Seed, A., Silks, D., Berry, L., Potts, R., Bell, I., Fox, N., Ebert, E., Eilts, M., O'Loughlin, K., Webb R., Carbone, R., Browning, K., Roberts, R. and

- Mueller, C. 2003. The Sydney 2000 World Weather Research Programme Forecast Demonstration Project: overview and current status. *Bull. Am. Met. Soc.* (in press).
- Liu, H. and Chandrasekar, V. 2000. Classification of hydrometeors based on polarimetric radar measurements: fuzzy logic and neuro-fuzzy systems, and in-situ verification. *J. Atmos. Oceanic Tech.*, 17, 140-64.
- Lopez, R.E. and Aubagnac, J.P. 1997. The lightning activity of a hail-storm as a function of changes in its microphysical characteristics inferred from polarimetric observations. *J. geophys. Res.*, 102, 16,799-813.
- May, P.T., Keenan, T.D., Zrnice, D.S., Carey, L.D. and Rutledge, S.A. 1999. Polarimetric radar measurements of tropical rain at C-band. *Jnl appl. Met.*, 38, 750-65.
- Mendel, J.M. 1995. Fuzzy logic systems for engineering: A tutorial. *Proc. IEEE*, 83, 345-77.
- Pruppacher, H.R. and Pitter, R.L. 1971. A semi-empirical determination of the shape of cloud and raindrops. *J. Atmos. Sci.*, 28, 86-94.
- Straka, J.M. and Zrnice, D.S. 1993. An algorithm to deduce hydrometeor types and contents from multiparameter radar data. *Preprints 26th Int. Conf. On Radar Meteorology*, Norman, OK, Am. Met. Soc. 513-515
- Straka, J.M., Zrnice, D. and Ryzhkov, A. 2000. Bulk hydrometeor classification and quantification using polarimetric radar data: synthesis of relations. *Jnl appl. Met.*, 39, 1341-72.
- Testud, J., Bouar, E.L., Obligis, E. and Ali-Mehenni, M. 2000. The rain profiling algorithm applied to polarimetric weather radar. *J. Atmos. Oceanic Tech.*, 17, 322-56.
- Vivekanandan, J., Bringi, V.N., Hagen, M. and Meischner, P. 1994. Polarimetric radar studies of atmospheric ice particles. *IEEE Trans GeoScience and Remote Sens.*, 32, 1-10.
- Vivekanandan, J., Zrnice, D.S., Ellis, S.M., Oye, R., Ryzhkov, A.V. and Straka, J. 2000. Cloud microphysics retrieval using S-band dual-polarization radar measurements. *Bull. Am. Met. Soc.*, 80, 381-8.
- Zrnice, D.S., Ryzhkov, A., Straka, J., Liu, Y. and Vivekanandan, J. 2001. Testing a procedure for automatic classification of hydrometeor types. *J. Atmos. Oceanic Tech.*, 18, 892-913.

